Plasma Sources Science and Technology

PAPER • **OPEN ACCESS**

Diagnosing asymmetric bipolar HiPIMS discharges using laser Thomson scattering

To cite this article: Marcus A Law *et al* 2021 *Plasma Sources Sci. Technol.* **30** 105019

OPEN ACCESS
IOP Publishing
Plasma Sources Science and Technology
Plasma Sources Sci. Technol. **30** (2021) 105019 (12pp)
https://doi.org/10.1088/1361-6595/ac2be4

Diagnosing asymmetric bipolar HiPIMS discharges using laser Thomson scattering

Marcus A Law, Francis Lockwood Estrin, Mark D Bowden and James W Bradley*

Department of Electrical Engineering and Electronics, University of Liverpool, Brownlow Hill, Liverpool L69 3GJ, United Kingdom

E-mail: j.w.bradley@liv.ac.uk

Received 18 August 2021, revised 21 September 2021
Accepted for publication 30 September 2021
Published 27 October 2021

Abstract

The temporal evolution of the electron temperature T_e and density n_e has been measured at two positions on the centre-line of an asymmetrically pulsed bi-polar HiPIMS plasma using incoherent laser Thomson scattering (LTS). The magnetron was operated with a tungsten target in argon atmospheres. The results show that in the plasma afterglow when positive voltage pulses are applied (above a threshold of at least 200 V) significant heating of the electrons can occur in which T_e can rise to values comparable to the those measured in HiPIMS on-time. The on-set of the rises in T_e are significantly delayed relative to the start of the positive pulse, with the delay time decreasing with the magnitude of the positive voltage. The delay is only weakly dependent on the operating pressure. The presence of large positive pulses can also affect the local electron density with n_e seen to decay significantly more quickly in the afterglow than for the corresponding unipolar pulsing case, in which no positive pulse is applied. The LTS measurements were complemented by a time-resolved study of the plasma optical emission (neutral argon and tungsten lines). With increasing positive potentials applied in the afterglow the Ar(I) line intensities grow consistent with increasing T_e. Interestingly, W(I) line intensities are detected in the afterglow with positive voltages $>$200 V despite the termination of all target sputtering, suggesting that tungsten is being re-sputtered from the vessel walls. With the aid of emissive probe measurements of the spatial and temporal evolution of plasma potential profile along the centre-line we discuss the phenomena of plasma electron heating and wall sputtering in the positive pulse. This is done in terms of the existence of a non-sustained reverse discharge, in which the vessel walls become an effective cathode.

Keywords: HiPIMS, bipolar HiPIMS, Thomson scattering, optical emission spectroscopy

(Some figures may appear in colour only in the online journal)

1. Introduction

High power impulse magnetron sputtering HiPIMS [1] is a relatively new physical vapour deposition technique that creates dense plasmas with large sputter ion fluxes through the application of low duty cycle but high energy density pulses to the target cathode. One advantage of this is that by biasing the substrate, the direction and energy of the sputtered ions that constitute the deposition flux can be controlled, producing films which are often harder, denser and smoother than those in comparable power DC magnetron sputtering [2–4]. It is well known that the deposition rate of HiPIMS is lower than that of its DC and pulsed-DC counterpart due to the back attraction of sputtered ions to the cathode target [5]. One potential method to counter this back attraction and aid transport of the metal ions to the substrate is to apply a positive voltage pulse to the target shortly after termination of the main negative

* Author to whom any correspondence should be addressed.

pulse (which creates the dense plasma), in technique known as asymmetric bipolar HiPIMS.

One of the first uses of bipolar pulsing in HiPIMS operation was by Nakano *et al* [6] in 2010, where a positive pulse was delivered for the full off-time of the discharge. It was found that the inclusion of a positive (reverse) target voltage in the afterglow significantly affected the discharge current rise-time of the subsequent on-time as the plasma ignition is suppressed due to the enhanced loss of charged particles. The first in depth study, utilising different positive pulse lengths and magnitudes to improve film qualities was made by Wu *et al* [7] in the deposition of Cu films on Si, in which they observed an increased deposition rate and reduction of tensile stress in the thin films when bipolar HiPIMS was used. Since that study, films produced using bipolar HiPIMS have been shown to have an increased density [8, 9], smoother surfaces [9, 10], improved hardness [8, 9], greater adhesion strength to the substrate [10] and a higher sp^3 content in diamond like carbon films [9, 11].

In the last few years, a number of important diagnostic studies have been performed to understand the basic plasma processes that lead to beneficial properties in thin films produced using asymmetric bipolar HiPIMS. A key tool has been energy-resolved mass spectrometry, which has revealed that the positive ion (argon and metal) kinetics are altered by the application of the positive pulse. From this, in general there is a generation of high energy ions at the substrate with upper energies corresponding to the applied positive voltage. For instance, Velicu *et al* [10] investigated the effect a positive pulse has on the time-averaged ion energy distribution function (IEDF) using a copper target in a balanced magnetron, observing two main energy peaks (at the substrate position); a low energy peak near zero energy and a high energy peak, corresponding to the applied reverse pulse magnitude which was not present in the unipolar pulses. Tiron and Velicu [12], extended the study to investigate the effect of positive pulse length on the ion kinetics and saw for short positive pulses, only a small fraction of copper ions gain energy but for increasing length, the ions gain successively more energy, with the count rate of the high energy peak increasing at the expense of diminishing ions at low energy. This effect was explained by the generation of a moving ion accelerating double layer structure that evolves in time. Such a structure joins two adjacent regions of positive and negative space charge and produces a potential profile with a characteristic step shape (see reviews [13, 14]). In bipolar HiPIMS using titanium targets Keraudy *et al* [15], found similar characteristic in the time-averaged IEDF's with Ti^+ and Ti^{2+} peaks at low energy corresponding to on-time ion generation and at high energy, corresponding to the positive target potential in the afterglow. A simple model of the potential structure in the discharge was also proposed, characterised by three distinct regions: the magnetic trap, a transition region, and the grounded region. Time-resolved IEDF's of Ti^+ ions were measured by Kozák *et al* [16], in which the magnitude of the high energy peak scaled with positive pulse length for duration less than 100 μs, with longer lengths yielding no additional benefits as the plasma had sufficient time to diffuse. They found that increasing the delay between the end of the negative pulse and initiation of the positive pulse affects the widths of the high energy peaks, with a district narrowing. Avino *et al* [17] found for niobium sputtering, long positive pulses (>250 μs) lead to the entire population of ions (Ar^+ and Nb^+) being shifted to higher energies. Detailed investigations of the time-averaged IEDF's of the sputtering of cobalt, in both reactive HiPIMS with argon and oxygen atmosphere mixtures [18] and HiPIMS with argon atmosphere [19] have been made, revealing differences between the cobalt and argon ions. High energy peaks, corresponding to the applied positive target potential was found for all species, with Co^+ showing a larger spread in energy than argon, thought to be due to the location in which the ions are created. Time-resolved IEDF measurements of the IEDF's in the sputtering of yttrium provide details on the appearance of different energy peaks [20].

Optical diagnostics have also been used on bipolar HiPIMS discharges. Laser induced fluorescence has been performed by Britun *et al* [21] to map the 2D density evolution of Ti^+ ground state ions in the positive pulse of a bipolar HiPIMS discharge. They found that during the positive pulse, a shrinkage of the ionisation region near the cathode is present, with fast ion acceleration from the cathode resulting in a faster redistribution of ions in the plasma than compared to the case with no positive pulse. Optical emission spectroscopy has yielded detailed information on the excited species during bipolar pulsing in which strong Ar(I) line emission is observed in the positive pulse indicating additional heating of the electrons and the formation a reverse discharge [16, 18, 20]. The authors suggest that two mechanisms may be at work: the generation of fast electrons returning to the positive target [16, 20], and the generation of secondary electrons from the chamber walls [20].

Time-resolved Langmuir probe measurements have shed light on the fundamental processes in bipolar HiPIMS discharges. For instance, it is observed that the floating and plasma potentials are raised rapidly on application of the positive pulse to values comparable to the target voltage and maintains this throughout the length of the positive pulse [16, 19]. Pajdarová *et al* [22] using a probe with sub-micro-second resolution showed that at the initiation of the positive pulse, large differences between plasma and floating potential were present, up to 200 V, indicating the generation of energetic electrons, confirmed by observation of short-lived hot electrons with temperatures up to 150 eV, derived from the probe characteristic. This process is simultaneously accompanied by a significant decrease in electron density. They also found that the average energy flux of ions to the substrate during the positive pulse increases with positive pulse height and shorter delay times between the negative and positive pulses.

Emissive probes have been used the determine the spatial and temporal evolution of the plasma potential in the bulk plasma of bipolar HiPIMS discharges. Interestingly, in some cases, during the positive pulse period, a distinct moving potential structure can be observed in the bulk plasma [10, 12]. These structures of raised positive potential at the rear and low potential at the head, advance downstream from cathode to substrate, with speeds of the order of the ion acoustic

speed. These features are indistinguishable from a classic double layer, with a distinct plasma potential step, that necessarily accelerates ions and electrons in opposite directions across the layer. The nature of the structure moving from cathode to anode will also enhance ion motion towards the substrate. However, these structures are not ubiquitous, for example, as aforementioned, Kozák *et al* [16], found that for an unbalanced magnetron, the plasma potential was raised very quickly some 100 mm from the target after initiation of the positive pulse indicating no moving structure. Hippler *et al* [19], and Pajdarová *et al* [22], found that both floating and plasma potential reaches high positive values at large distances from the cathode in a similar fashion. It is conjectured by Tiron and Velicu [12] that the plasma and magnetic topology of the device may influence the response of the plasma potential in the positive pulse period and the possible development of a moving double layer in the plasma during the positive pulse. They suggest that short negative HiPIMS pulses followed by highly positive short pulses are favourable for a double layer formation, as an effective ion acceleration mechanism. Kozák *et al* [16] suggest that no layer will be found in strongly unbalanced magnetron configurations, in which the fast electrons outside of the magnetic trap can reach the biased target with ease, so equilibrating and raising the potential quickly in the bulk. Currently, it is still difficult to predict whether moving potential structures will appear in a particular magnetron during bipolar operation.

Despite the excellent work to date in measuring the plasma parameters in asymmetric bipolar HiPIMS plasmas, many of the probe and analysis techniques can be highly perturbing to the plasma, thus affecting the results, or making interpretation difficult. In this study, the temporal evolution of electron properties on the centre-line of the magnetron has been determined using LTS for a range of argon pressures and positive voltage profiles, namely positive pulse height and duration. The LTS technique is non-intrusive, which in the limit of incoherent scattering [23], allows the determination of the electron temperature T_e through acquisition of the electron velocity distribution function and electron density n_e from the intensity of the scattered radiation. Interpretation of the obtained LTS spectra is straightforward. LTS has been used recently to determine the time-evolution of electron properties in HiPIMS [24–26] and DC [25] magnetron discharges. To our knowledge this is the first LTS study of the asymmetric bipolar HiPIMS plasma, and we concentrate on how the positive pulse affects the electron density and temperature during the afterglow period. The LTS studies are complemented by optical emission spectroscopy to determine the temporal evolution of the important gas and metal ion emission line Ar(I) and W(I). In addition, emissive probe measurements have been made of the temporal evolution of axial plasma potential during the entire bipolar HiPIMS period, to aid understanding of the basic processes inferred from the LTS and optical emission studies.

2. Experimental arrangement, plasma source and diagnostics

The experimental arrangement, including the vessel, magnetron and LTS system is shown in figure 1(a). This system is described in [25, 26]. The plasma source consists of a 150 mm diameter planar unbalanced magnetron (Vtech 150 from GENCOA Ltd), fitted with a tungsten target of purity >99.95%. The chamber was pumped down to a base pressure of 2×10^{-3} Pa using a turbo molecular (Pfeiffer TMU071P) and rotary pump (Edwards RV3) set. Argon gas of purity >99.99% was introduced to the chamber using a mass flow controller (MKS 1179 A). In this study diagnostic measurements were taken at two pressures, 0.8 and 1.6 Pa. Figure 1(b) shows the unbalanced magnetron B-field topology (lines) and the two LTS measurement positions on the centre-line at $z = 61$ mm and $z = 15$ mm. The measurement position $z = 61$ mm lies at the magnetic null point.

Discharges were driven by a home-made asymmetric bipolar HiPIMS power supply consisting of two synchronised generators, one for generating conventional negative voltage pulses (to -1 kV) and the second for generating reverse polarity positive voltage pulses (to $+350$ V), delayed by 8 μs after termination of the former.

The target voltage and current waveforms were measured using a 100× Tektronix P5100 voltage probe and a model 110 A Pearson current monitor respectively. Figure 2 shows example voltage and current waveforms for a variation of positive voltages and durations, with in each case an average pulse energy, power, and peak target power density of 1.8 J, 85 W–230 W cm^{-2}. All discharges used in this work had a fixed repetition rate of 50 Hz and negative pulse length of $t_{np} = 50$ μs.

One can see from figure 2 that increasing the positive pulse voltage and duration can marginally increase the current rise time and reduce the peak current during the negative pulse (main sputtering phase). As we will show later this may be due to lower residual electron densities being available in the afterglow to aid ignition of the next pulse when large positive pulses are utilised. The insert plot for current shows reverse negative currents of up to about 5 A to the cathode are generated when positive voltages are applied.

The Thomson scattering diagnostic used to determine the electron density and temperature at the two positions denoted by $z = 61$ mm and $z = 15$ mm in figure 1(b) is described fully in [25, 26]. Briefly it consists of a Quantel Brilliant B laser operating at repetition rate of 10 Hz and frequency doubled to emit radiation at 532 nm, with an energy of 240 mJ. The scattered light was collected using a lens of focal length 200 mm and directed into the Horiba T64000 triple grating spectrometer with an Andor iSTar iCCD detector. The electron velocity distribution function is in an arbitrary direction to the target surface plane in the measurement volume. We can assume on the centre-line the velocity distribution is isotropic. The entrance slit of the spectrometer was set to 0.3 mm, providing an image on the detector of the detection volume of dimensions, $3.3 \times 0.17 \times 0.25$ mm^3. Since the magnetron anode ring protruded ~7 mm from the target surface we made measurements no less than 15 mm from the target to minimise stray light reflections entering the detection system. Time-resolved measurements required that the laser, iCCD and plasma source were synchronised. This was achieved by using a TTL signal from the HiPIMS source to trigger the firing of the laser which

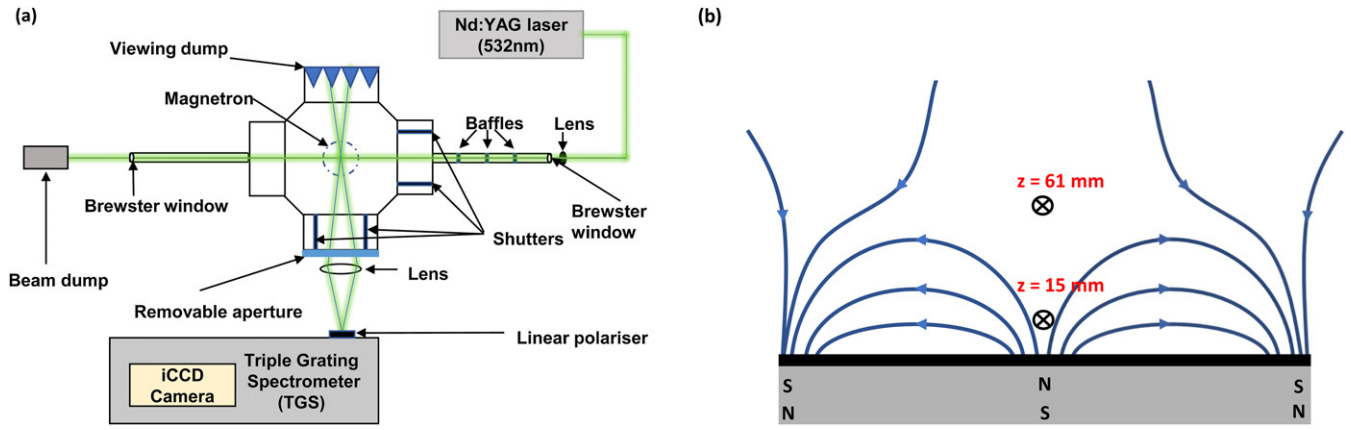

Figure 1. Top view schematic of the experimental apparatus (a) and a side view of the magnetron and representative magnetic field lines (b). The points $z = 61$ mm and $z = 15$ mm on the centre-line indicate the positions of the scattering volume from which light was viewed.

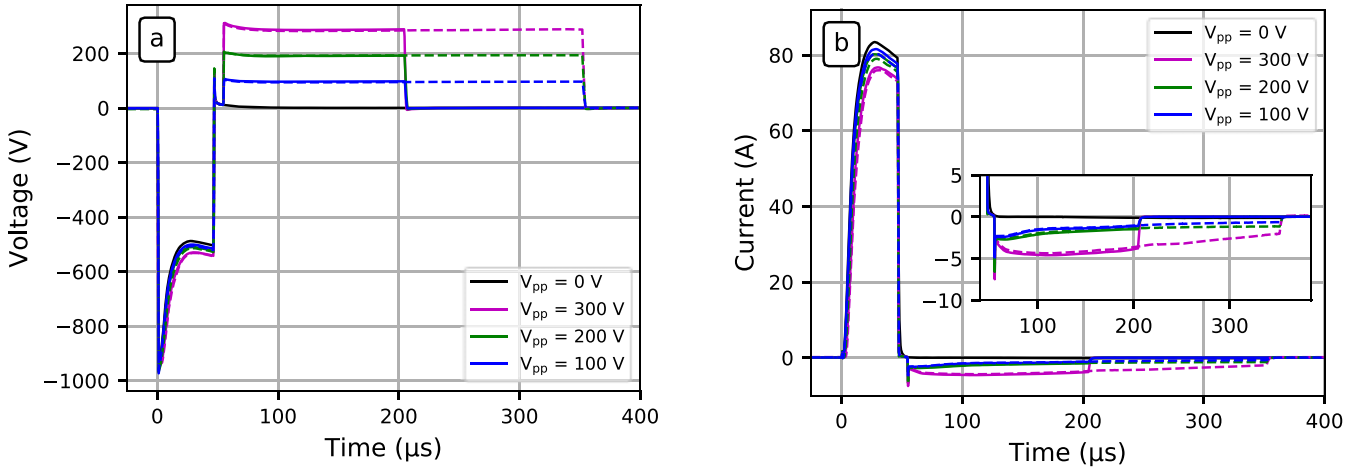

Figure 2. Example discharge voltage (a) and current (b) waveforms. The black curve represents the waveform of an uni-polar pulse of width 50 μs. Blue, green and magenta curves represent discharges with 150 μs (solid line) and 300 μs (dashed line) duration positive pulses of 100, 200 and 300 V respectively. The pulse cycle repetition rate is 50 Hz with an operating pressure of 1.6 Pa.

in turn triggered the iCCD. The laser pulse was delayed in time through the use of an Arduino board and the 50 Hz signal was divided by 5 to produce the 10 Hz signal for the laser. This system had a time resolution of ~5 μs. Spectral data was accumulation over 600–2400 laser pulses (60–240 s) with a gate width set to 7.5 ns.

An example scattered light spectrum obtained in this study is shown in figure 3, taken in the positive voltage phase of a HiPIMS period. The spectral resolution of the system was approximately 0.071 nm. The data outside of the notch filter region (531.5–532.5 nm) is fitted to a Gaussian function to obtain the electron temperature [27]. In this arrangement, the instrument could resolve electron temperatures down to 0.12 eV, and hence measurements into the deep afterglow of the HiPIMS pulse were not possible. Typical errors on the measured T_e values are in the range 2%–6%, found from the standard deviation of the Gaussian fit parameters. The absolute electron density was obtained through a calibration procedure by means of Rayleigh scattering from room temperature argon gas of a known density [27]. Typical errors on the measured n_e values are in the range 2%–10% found from the standard deviation of multiple Rayleigh scattering measurements at several pressures and propagation of errors from the Gaussian fit from the TS spectra.

Optical emission line data from the discharges was also obtained using the triple grating spectrometer, however in this case with a small aperture of diameter 3 mm placed behind the collection lens to limit the solid angle of collection and the entrance slit changed to 0.1 mm to improve the spectral resolution. The emission line measurements were synchronised by the TTL signal from the HiPIMS generator, and the internal clock of the camera provided the necessary delay from the start of the pulse. The ICCD detector was gated for 5 μs at 50 Hz and data was accumulated over 20 s (1000 pulses) for both background and plasma measurements. The study concentrated on emission lines in neutral argon at 751.47 nm (transition $3s^23p^5(^2P^0_{3/2})4p \rightarrow 3s^23p^5(^2P^0_{3/2})4s$) and tungsten at 484.38 nm (transition of $5d^46s(^6D)6p \rightarrow 5d^46s^2$) An example spectrum for tungsten is shown in figure 4, Assuming a Gaussian fit to the line, a relative intensity could be calculated.

The emissive probe used in this study is described in [28]. Briefly, it consists of a 50 μm diameter thoriated tungsten wire push-fitted into the probe stem, forming a semicircle protruding 2 mm, heated until full electron emission was achieved, by

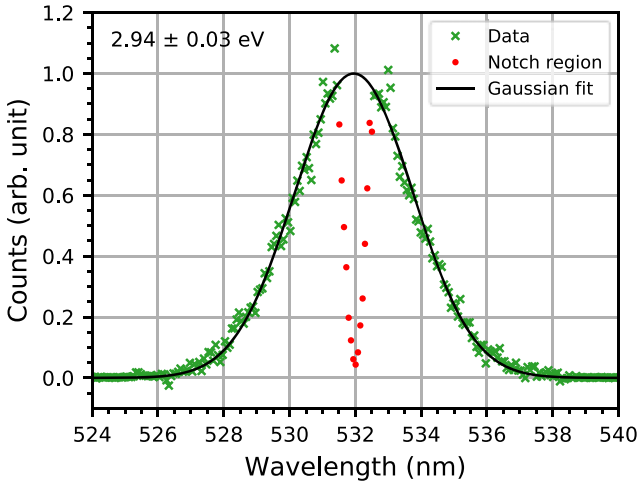

Figure 3. Example high temperature LTS spectra measured at $z =$ 15 mm from the target surface at 265 μs from the HiPIMS initiation in the positive pulse domain of magnitude 300 V and length 300 μs. Here the measured temperature is 2.94 $\pm$ 0.03 eV deduced from a Gaussian that was fitted to the data outside the notch filter region.

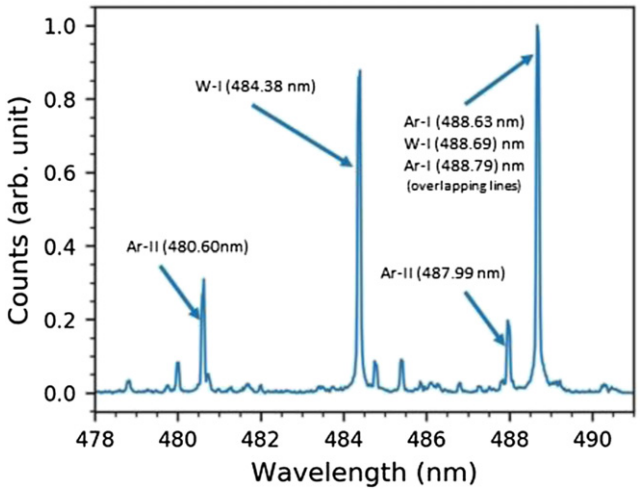

Figure 4. An example optical emission spectrum for emission lines in the region 478 nm–491 nm taken at 10 μs into a HiPIMS pulse. Highlighted is the wavelength of interest of W–I at 484.38 nm and several other strong emission lines in this region.

a 50 Hz ac current supplied by a transformer circuit with current of 0.62 A. The probe had a spatial resolution of $\sim$2 mm and had a temporal resolution of below 20 ns [28]. The error in the plasma potential measurement was of the order of the voltage equivalent of the surface temperature $<$0.25 V. The emissive probe was fixed at one position relative to the chamber walls and the magnetron was moved vertically up or down to allow measurements to be made at different axial positions on the centre-line.

3. Results

In this study, measurements of electron plasma properties, plasma emission and plasma potential were made for a range of discharge conditions, in order to understand the effect of the positive pulse on plasma behaviour. Plasmas were struck at two pressures, 0.8 Pa and 1.6 Pa (typical HiPIMS operating pressures). The pulse frequency was held at 50 Hz and the on-time t_{np} was kept constant at 50 μs. The positive voltage pulse durations and heights were varied, namely $t_{\mathrm{pp}} = 150$ μs and 300 μs and $V_{\mathrm{pp}} = 0$, 100, 200 and 300 V respectively. $V_{\mathrm{pp}} = 0$ V case is just the normal unipolar HiPIMS case where no reverse pulse was added to the voltage signal. The delay between the negative and subsequent positive pulse was 8 μs.

The results are presented in three sub-sections, which describe measurements of plasma electron properties, optical emission and plasma potential, respectively. For both the Thomson scattering and optical emission measurements light was focussed from regions on the discharge centre-line at $z =$ 15 mm and at $z = 61$ mm from the target and the emissive probe scanned the plasma potential over a region on the centre-line.

3.1. Temporal evolution of T_e and n_e

In this section, the results of LTS measurements are presented in order to understand how the addition of the positive voltage pulse affected the temporal evolution of the electron plasma properties. Figure 5 shows the temporal evolution of T_{e} and n_{e} at the position of the magnetic null, $z = 61$ mm with $t_{\mathrm{pp}} = 150$ μs for the four V_{pp} cases. From figure 5(a), we clearly see a rise in temperature in the positive pulse period for the $V_{\mathrm{pp}} = 300$ V case, with T_{e} starting to rise about 120 μs after positive pulse ignition from 0.44 eV to a peak of 0.93 eV. No such increase is seen for the other two positive pulse cases. This electron heating is rapidly terminated as the target is grounded at the end of the reverse voltage period at $t = 208$ μs and is followed by cooling but with T_{e} values always higher than the other V_{pp} cases. These higher T_{e} values in the long afterglow are accompanied by lower electron densities as shown in figure 5(b). That is, the density of these hotter electrons is decaying much faster once the target voltage rapidly transitions from a finite V_{pp} value to ground.

Figure 6 shows what effect a lengthening of the positive pulse period had, with t_{pp} increased to 300 μs, with all the other operating conditions remaining fixed. In the $V_{\mathrm{pp}} = 300$ V case, electron heating can now persist for longer with T_{e} peaking at $t \sim 180$ μs with a value of $\sim$2.6 eV. This is followed by slow cooling in the remainder of the positive pulse period and the long afterglow. In contrast to results in figure 5 the $V_{\mathrm{pp}} = 200$ V now does reveal a T_{e} rise but much delayed compared to the $V_{\mathrm{pp}} = 300$ V case. The T_{e} heating is terminated by the end of the positive voltage period. We quite clearly see that the higher the positive pulse voltage the sooner the T_{e} rise occurs. For positive pulse voltages of $V_{\mathrm{pp}} = 100$ V no T_{e} rise is seen at all, although this may happen for much longer t_{pp} durations not explored here. The electron density–time curves in figure 6(b) show that in the cases where electrons are heated their densities decrease more rapidly in the long afterglow, the phase where the target voltage goes to ground. Interestingly, there is a pronounced sharp dip in n_{e} in the afterglow $t = 250$ μs when the positive pulse of 300 V is applied. Figure 6 reveals that with high V_{pp} values i.e. 300 V, the electron temperatures

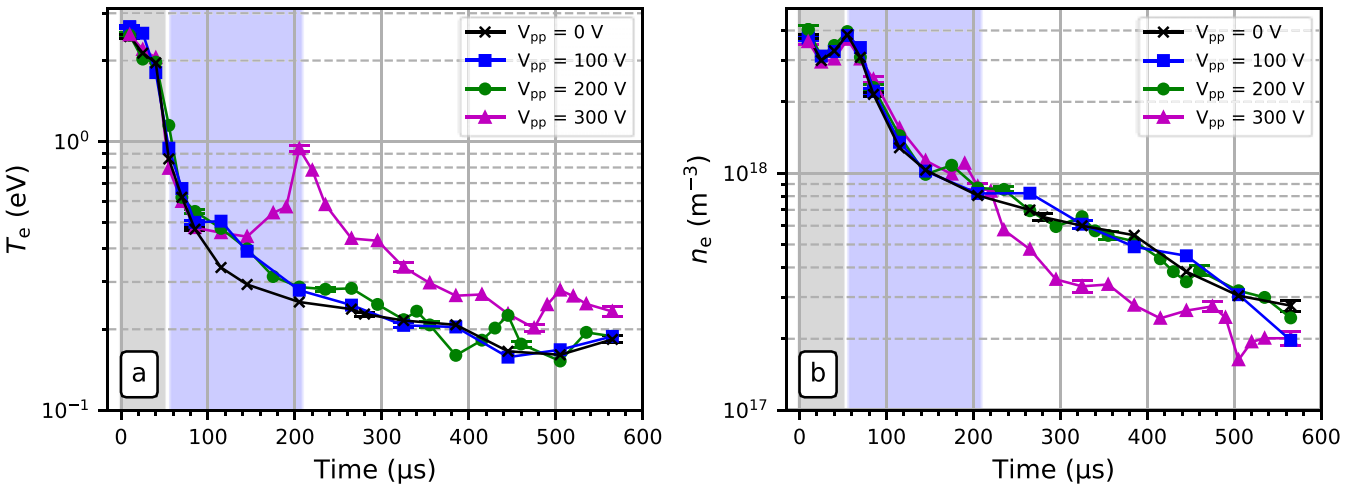

Figure 5. Plots of (a) the electron temperature T_e and (b) electron density n_e versus time at position $z = 61$ mm, for a negative pulse duration of $t_{np} = 50$ μs (grey region), positive pulse duration of $t_{pp} = 150$ μs (blue region) for $V_{pp} = 0$, 100, 200, and 300 V. The operating pressure was 1.6 Pa.

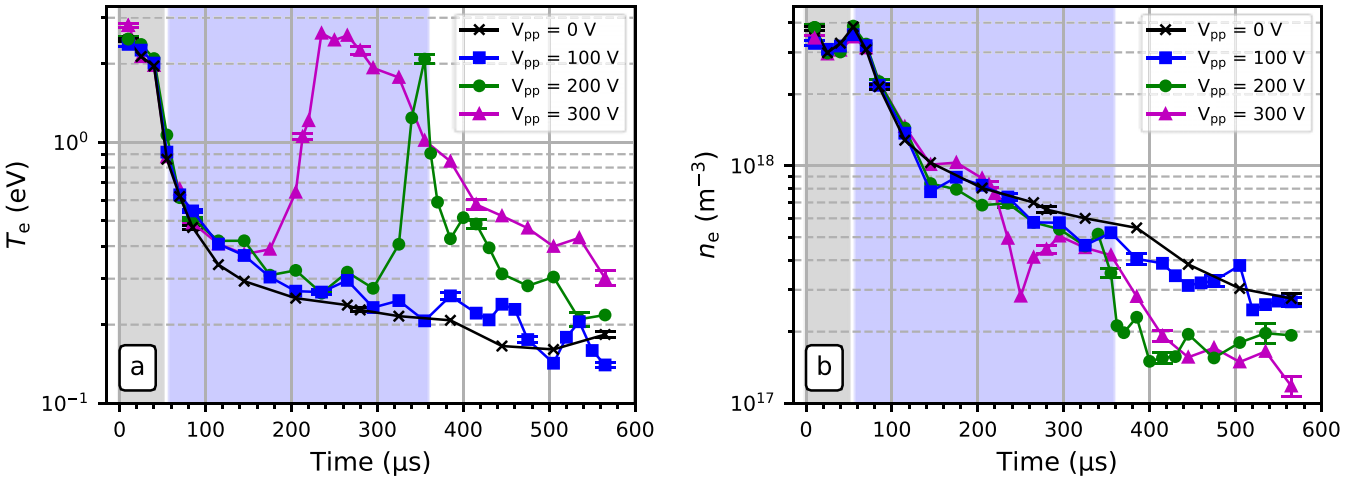

Figure 6. Plots of (a) the electron temperature T_e and (b) electron density n_e versus time at position $z = 61$ mm for the same operating conditions as in figure 5 but with a positive pulse duration increased to $t_{pp} = 300$ μs.

in the whole of the afterglow are significantly raised compared to the conventional unipolar equivalent pulse where $V_{pp} = 0$.

The effect of halving the pressure from 1.6 Pa to 0.8 Pa on the T_e and n_e temporal profiles at position $z = 61$ mm is shown in figure 7 for the two positive pulse lengths, t_{pp} of 150 and 300 μs and $V_{pp} = 300$ V. We see that high pressures lead to higher on-time electron densities (increase of 20%–30%) and lower electron temperatures at the end of the negative pulse (2.0 eV as opposed to 2.4 eV) as we may expect. For cases with no positive pulses applied ($V_{pp} = 0$ V), the electron temperatures are lower in the afterglow for the lower pressure. With the application of a positive pulse, the peak in electron temperature is delayed for higher pressure case and for $t_{pp} = 300$ μs, the heating at higher pressure takes longer to decay compared to the lower pressure discharge. After termination of the positive pulse, densities at both pressures decay quicker in comparison to the unipolar ($V_{pp} = 0$ V) case, with the $P = 0.8$ Pa showing the most exaggerated drop in density, thought to be due to the fact that there are less collisional processes, meaning the plasma can diffuse and escape the target vicinity.

The spatial variation of T_e and n_e were explored by making measurements closer the magnetron target, namely at position $z = 15$ mm, a scattering volume also on the discharge centreline. This is the closest possible distance to the magnetron without suffering a significant stray light increase due to light reflections from the magnetron anode ring. Figure 8 shows the measured $z = 15$ mm position values of T_e and n_e values at an operating pressure of 1.6 Pa with $t_{np} = 50$ μs, $t_{pp} = 300$ μs for $V_{pp} = 0$ and 300 V. Plotted together on the same axis are those at $z = 61$ mm as a comparison (this data is also shown in figures 6 and 7). At the closest distance to the target, for the $z = 15$ mm position, T_e is much lower during the negative driving pulse region of the HiPIMS discharge than those measured at $z = 61$ mm irrespective of the positive pulse conditions, with T_e peaking at about 1 eV rather than ~2.4 eV. However, just into the afterglow regions (first 50–100 μs) in all cases the T_e values become comparable and decay similarly. As seen at

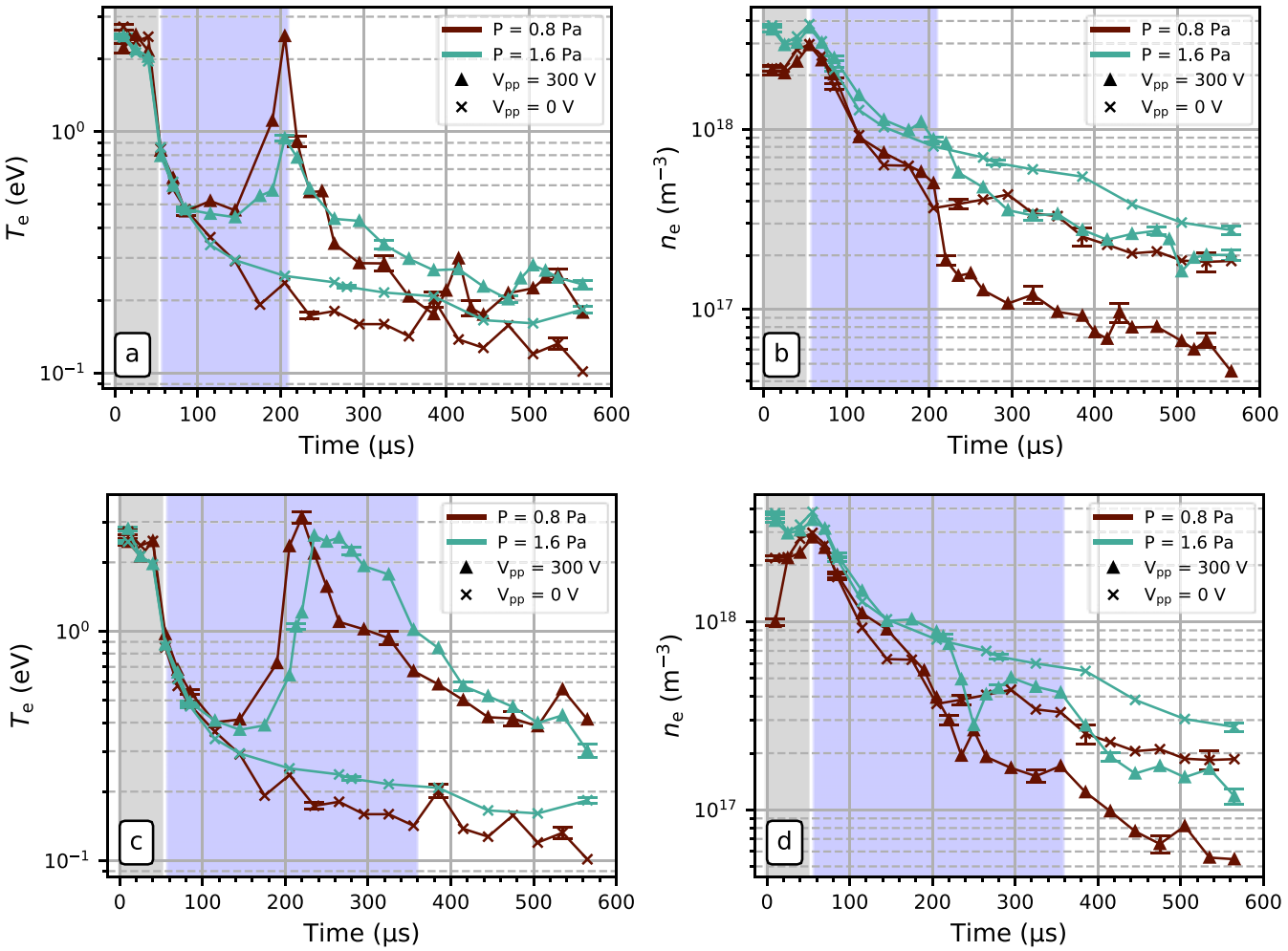

Figure 7. (a)–(d). Plots of the electron temperature T_e (a) and (c) and electron density n_e (b) and (d) versus time measured at position $z =$ 61 mm for a variation of positive pulse length and operation pressure. $t_{pp} = 150$ μs for plots (a) and (b). $t_{pp} = 300$ μs for (c) and (d). The two operating pressures are indicated in the legend.

position $z = 15$ mm with a positive pulse of $V_{pp} = 300$ V significant transient electron heating is seen with T_e values peaking at 3 eV, a value marginally higher, but slightly delayed in time compared to measurements at $z = 61$ mm. As aforementioned, the electron density measurements for the $V_{pp} = 300$ V positive pulse case, measured at $z = 61$ mm, shows an unusual sharp dip in the afterglow at $t = 250$ μs, it somewhat mirrors the sharp peak in n_e at 270 μs seen in the same discharge measured at $z = 15$ mm. If these features are related it shows an effect happens first at the magnetic null, then close to the target.

3.2. Temporal evolution of Ar and W optical emission lines

In this section, optical emission spectroscopy results are presented to complement the electron property results and to shed light on the main physical processes occurring in the positive pulse regions of the bi-polar pulse regime, the study was conducted focussing on the dominant neutral lines for electronically excited argon, Ar(I) ($\lambda = 751.47$ nm) and tungsten W(I) ($\lambda = 484.38$ nm). No significant lines from ionised species Ar(II) and W(II) were detectable outside the negative pulse period of the HiPIMS discharge. To minimise the transmission loss due to sputtering, the acquisition time was kept low and to quantify the intensities, each spectrum was normalised to the maximum intensity of the temporal scan of the particular species to produce a relative intensity for each.

Figure 9 shows the Ar(I) and W(I) relative intensities for (a) at position $z = 15$ mm and (b) at position $z = 61$ mm for the discharge conditions of $t_{np} = 50$ μs, $V_{pp} = 300$ V, $t_{pp} = 300$ μs with operating pressure of 1.6 Pa. Also plotted here is the LTS obtained electron temperature for the two corresponding discharges for comparison. During the negative voltage region of the HiPIMS pulse, the W(I) line intensity increases and the Ar(I) line decreases as the pulse evolves in time, consistent with the expected transition from an argon gas to tungsten metal dominated discharge regimes. It is clear from the plots at both positions that the Ar intensity profile follows the electron temperature. As T_e peaks in the positive pulse period so does the Ar line intensity. During this phase the electron density is falling (see figure 6) while the background neutral argon density is expected to increase as the argon streams back into the target region after rarefaction in the negative pulse [29]. This is evident in figure 9, between times 100 and 200 μs as Ar increases while T_e decreases. The greater excitation of neutral

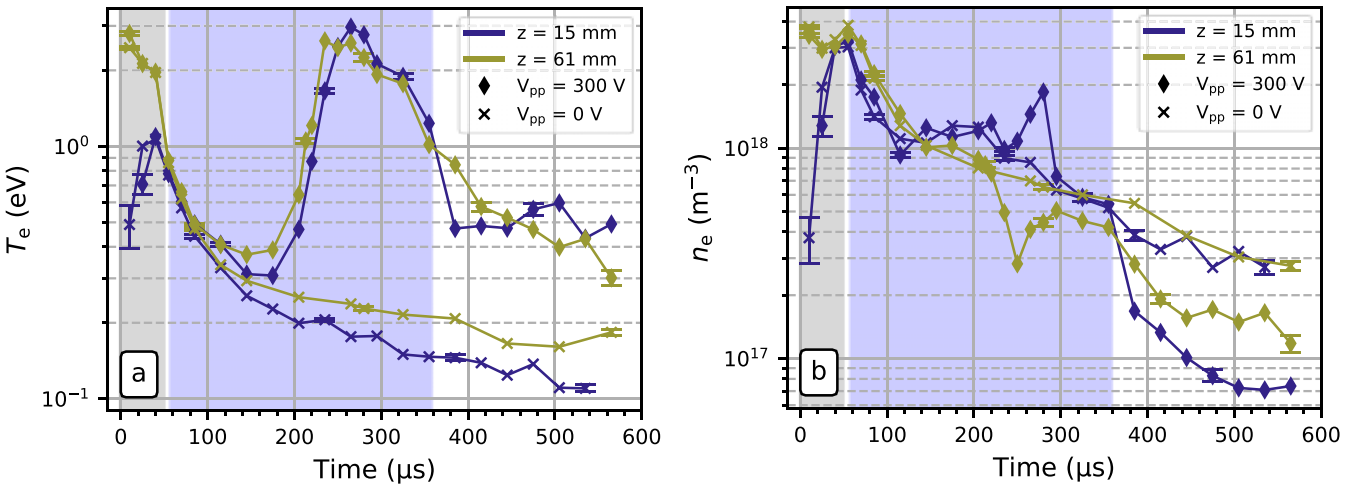

Figure 8. Plots of the electron temperature T_e (a) and density n_e (b) versus time measured at position $z = 61$ mm and $z = 15$ mm, for $t_{pp} = 300$ μs for $V_{pp} = 0$ and 300 V at an operating pressure of 1.6 Pa.

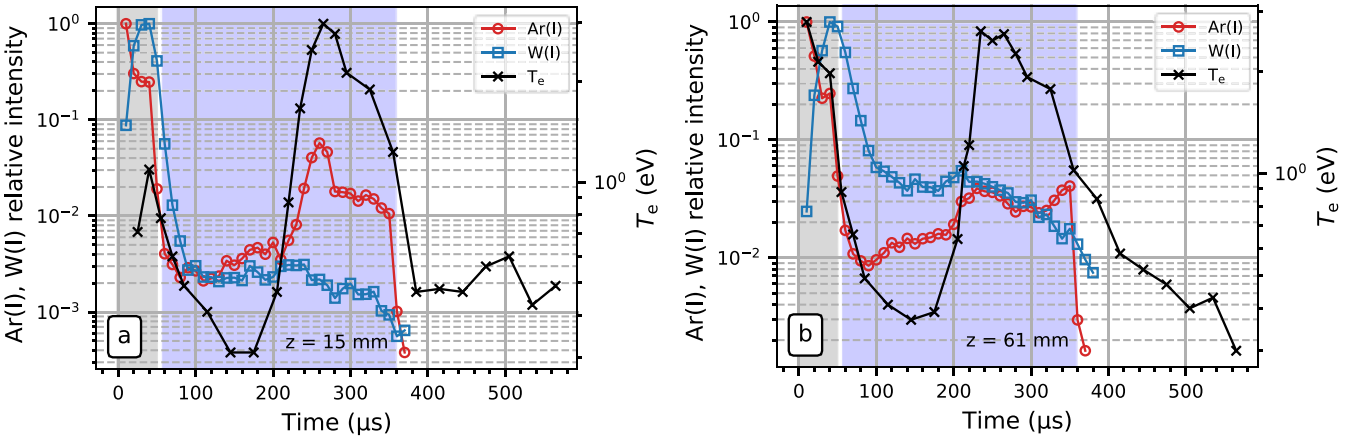

Figure 9. A plot of the temporal evolution of the Ar(I) and W(I) line intensities at $z = 15$ mm (a) and $z = 61$ mm (b) respectively together with the LTS obtained electron temperature for the case $V_{pp} = 300$ V, $t_{pp} = 300$ μs with a pressure 1.6 Pa obtained at positions $z = 15$ mm and $z = 61$ mm.

argon by hotter afterglow electrons despite the fall in n_e leads to more light intensity. Just after termination of the positive pulse when the electrons cool rapidly the Ar(I) emission falls almost instantaneously below the threshold for detection.

The behaviour of the W(I) line intensity is somewhat different. It is constant during the first half of the positive pulse but as T_e rises it decreases (unlike Ar(I) emission) before falling to undetectable levels immediately after the positive pulse termination. This indicates that the neutral tungsten density may be falling during the same period as T_e rises. However, line intensities are very sensitive to changes in electron density and since n_e is falling in the same period, it is hard to speculate on exactly why the W(I) line intensities fall during electron heating. In a number of HiPIMS experiments, it was found that thermalised metal atoms can remain in the discharge for considerable periods, in the afterglow (see for example [30]). However, we argue that most of the W atoms coming from the sputtering period will have exited the discharge within 40 μs. This was found from a simple calculation based on the most probable kinetic energy of sputtered neutrals to be half the surface binding energy of 11.8 eV [31] travelling a distance of 10 cm from the target. We suggest that the source of W is from the grounded vessel walls. During the on-time, target sputtered W will deposit on the walls. During the positive pulse period, the plasma potential is elevated to a value close to V_{pp} and so argon ions from the plasma can effectively sputter the walls through energetic bombardment, in the case shown in figure 9 with energies up to 300 eV. As the argon ion densities decay in the positive pulse period, where the plasma is not sustained from target processes, any new source of W from the sputtering of chamber wall material must necessarily fall. It is important to note that without the positive pulse present, no significant trace of Ar or W emission is detected in the afterglow.

Energetic argon ion bombardment of the walls in the positive pulse period of the afterglow will liberate secondary electrons that are sheath accelerated to enter the plasma with energies equivalent to V_{pp} and become thermalised in the decaying plasma. We argue that these secondary electrons sustain and heat a reverse discharge for some 100 μs or so

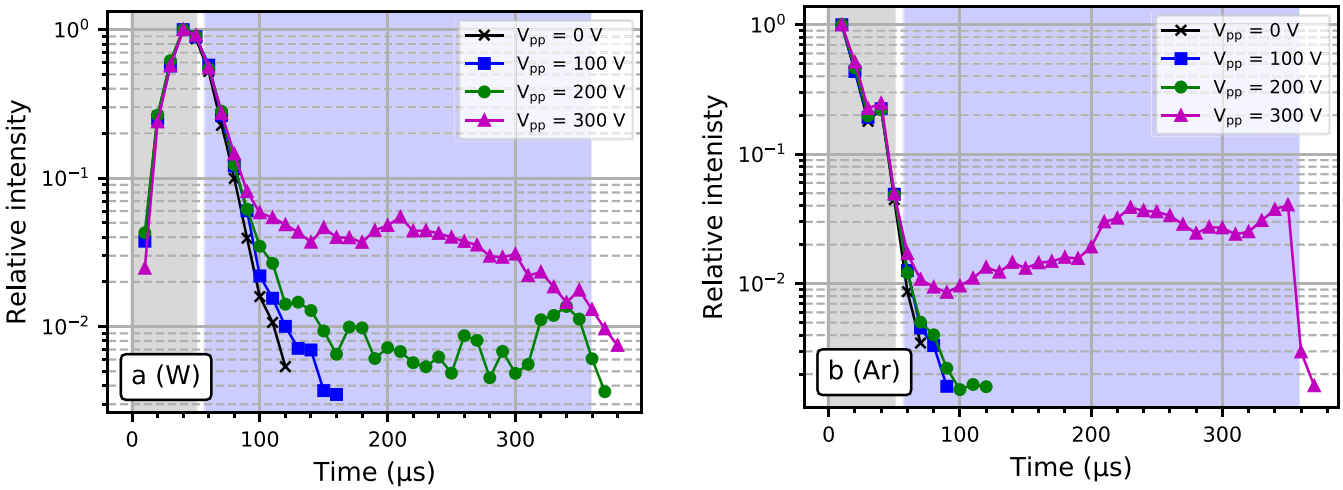

Figure 10. A plot of the temporal evolution of (a) W(I) and (b) Ar(I) line intensities at 484.38 nm and 751.47 nm respectively for $t_{pp} = 300$ μs for changing positive pulse voltages $V_{pp} = 0$, 100, 200 and 300 V and $P = 1.6$ Pa measured at position $z = 61$ mm.

before the plasma has time to significantly decay. The reverse discharge is clearly not self-sustaining.

To investigate if the wall sheath potentials can, in the positive pulse period, influence the short-lived wall (re)sputtering and secondary electron release (leading to bulk heating) the temporal W(I) and Ar(I) intensities have been plotted for $V_{pp} = 0$, 100, 200 and 300 V in figures 10(a) and (b) respectively.

In the absence of a positive pulse ($V_{pp} = 0$) both Ar(I) and W(I) lines decay quickly in the afterglow falling below the detection limit at $t \sim 120$ μs. The $V_{pp} = 100$ V is similar however, W(I) emission persists to $t \sim 150$ μs. For higher positive pulse voltages, the W(I) line intensities remain strong for the whole pulse period with $V_{pp} = 300$ V revealing a larger signal consistent with broader peak T_e values as shown in figure 6(a). The gradual decay in W(I) line intensity is consistent with a decay in the density of source tungsten atoms originating from the walls in the afterglow plasma. Ar(I) emission is only seen in the positive pulse period for the $V_{pp} = 300$ V case, a situation where transient but significant electron heating is occurring in the plasma.

To examine what effect pressure has on the intensity of excited species in the discharge, measurements were performed at a lower pressure of 0.8 PA as used previously in the LTS study. Data was collected at position $z = 61$ mm and figure 11 shows the effect of changing pressure on the chosen emission lines. For the 0.8 Pa case, the W(I) emission in the positive pulse becomes undetectable at ~220 μs whereas at 1.6 Pa it persists through the positive pulse. The Ar(I) plot shows that at both pressures, the emission is present in the positive pulse and increases towards the end before falling to zero after the positive pulse termination.

3.3. Temporal evolution of plasma potential through the positive pulse

In this section, the results of an emissive probe scan, tracking the plasma potential along the centre of the magnetron axis at regular intervals are shown. The measurements were taken from 20 mm from the target surface and extended to a 70 mm distance in steps of 5 mm. It should be noted here that the probe had a fixed position, and the magnetron was moved vertically in the chamber relative to the fixed probe.

Figure 12(a) shows the temporal evolution of the plasma potential at several positions during a bipolar HiPIMS discharge with a 300 μs, 300 V positive pulse. During the early stages of the positive pulse, the plasma potential rises sharply at all positions taking around 10 μs to reach the target potential. Soon after, the measured plasma potential at each position exceeds the target potential by several volts. Figure 12(b) shows a contour plot of the early stages of the positive pulse (where one would expect a double layer to form if present). It is clear from this plot that the plasma potential rises almost uniformly across all the measured positions with little to no delay at each position, indicating no significant structure is present along the measured positions.

4. Discussion

With application of a positive pulse in the discharge afterglow, we measure at two positions along the centre-line a distinct transient rise and decay in electron temperature. The rise is seen to be delayed relative to the initiation of the positive pulse. The maximum acquired electron temperatures are more pronounced for longer positive pulse lengths and the delay in electron heating is shortened with increasing magnitude of positive pulse voltage.

A two-fold increase in the gas pressure has only a marginal effect on the degree and timing of the electron heating phenomenon. The plasma to which the positive pulse is applied is essentially a decaying afterglow, as shown in all cases by the falling electron densities much the same as in the normal 'off-time' of unipolar HiPIMS operation.

In the positive pulse phase, the emissive probe measurements (figure 12) show that the plasma potential is raised rapidly at all positions along the centre-line. The bulk plasma then necessarily sits at a high potential relative to the grounded

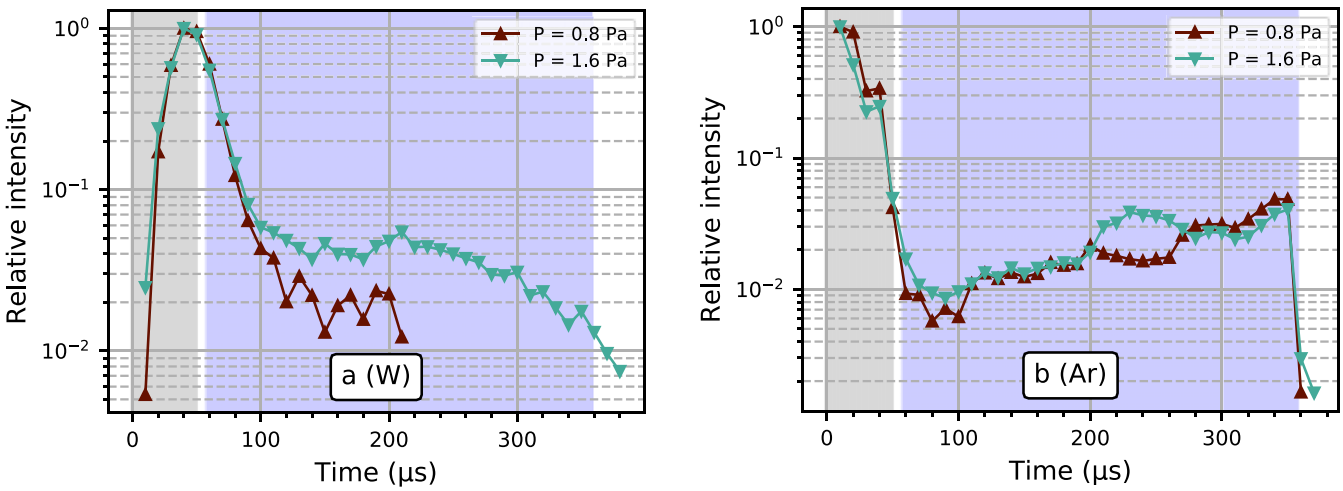

Figure 11. A plot of the temporal evolution of (a) W(I) and (b) Ar(I) line intensities at 484.38 nm and 751.47 nm respectively for $t_{pp} = 300$ μs for changing pressure for $V_{pp} = 300$ μs.

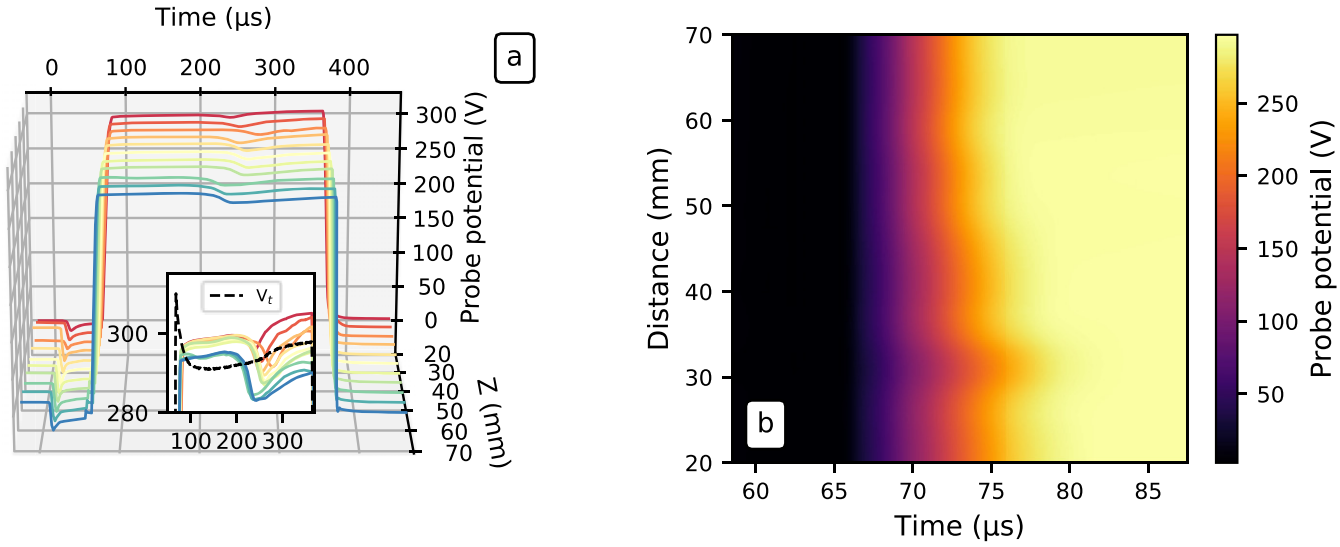

Figure 12. A plot of the temporal evolution of the (a) the plasma potential profile throughout a $V_{pp} = 300$ μs, 300 V bipolar HiPIMS discharge ignited at 1.6 Pa of argon gas at several distances from the target. The target potential V_t is also plotted for comparison. (b) A contour plot of the early stages of the positive pulse.

vessel walls, making the walls an effective cathode. Plasma ions will be accelerated across the wall sheaths (up to 300 V in this study) to both sputter the walls and liberate secondary electrons. We can call this phase a 'reverse' discharge, however it is clearly non-self-sustaining since the plasma continues to decay.

The optical emission study shows a measurable concentration of tungsten in the discharge during this 'reverse' phase, thought to be, in part due to the re-sputtering of a thin layer of tungsten from the walls and excitation of slow, low energy target liberated tungsten left over from its creation in the on-time, excited by the newly elevated electron temperature. The W(I) emission signal however decays, presumably due to the continuous reduction in the number of argon ions available to sputter the walls and the continuous loss of long lived, on-time tungsten, as the whole bulk plasma decays. At termination of the positive pulse, the W(I) line and Ar(I) intensity drops very rapidly, as the wall sheath potential and any W re-sputtering collapses.

The observed transient electron heating during positive pulses (for amplitudes greater or equal to 200 V) may be explained in terms of the creation of secondary emitted electrons at the wall. These electrons will be accelerated across the wall sheath, losing energy through inelastic collisions with bulk plasma species and thermalising to form an effectively hot group with a distribution of energies indistinguishable from a Maxwellian. The slowing down and thermalisation (equipartition) times for sheath accelerated secondary electrons in the bulk plasma can be calculated following an expression stated in Spitzer [32]. For example, if we assign an effective energy of $T_e = 300$ eV to sheath accelerated secondary electrons (in

the case described in figure 6), then on initiation of the positive pulse and entering the bulk plasma of electron density $\sim 10^{18}$ m^{-3} and temperature $k_B T_e/e$ of $\sim$1 eV, these electrons will have a slowing down time $\tau_s \sim 70$ μs and equipartition time $\tau_{eq} \sim 100$ μs. From figures 5 and 6, we see that given sufficient duration of the off-time period and for $V_{pp} \geqslant 200$ V, we see a distinct peak in T_e in the positive voltage period. It is difficult to know exactly why the temperature peaks however, the energy flux of secondary electrons acting as a source of heating in the bulk is reduced during the afterglow. With a decaying source of energy this may lead to a peak in electron temperature.

Wall-sheath accelerated secondary electrons generated in the positive pulse may not necessarily acquire the background bulk electron temperature but heat the plasma locally to form a hot group as observed in the LTS measurements. These electrons must necessarily cross open magnetic field lines of the relatively weak field downstream of the target to reach the measurement point, undergoing collisions with neutral gas, taking a finite time to do so. This time can be estimated by simple consideration of the classical cross-field diffusion coefficient of particles across B fields, given by

$$D = \frac{k_B T_e}{m_e \upsilon \left(1 + \omega_c^2 \tau^2\right)},$$

where τ is the average collision time (inverse of the momentum stopping collision frequency, calculated using the cross-section for collisions and electron thermal speed), ω_c is the gyro radius given by $\frac{qB}{m}$. In the limit $(\omega_c \tau)^2 \gg 1$ (valid in this study), this expression reduces to

$$D = \frac{k_B T_e \upsilon}{m_e \omega_c^2}$$

and the time for electrons to traverse distance L across the field can be stated as $\tau_D = L^2/D$.

If we assume a heated population of $k_B T_e/e = 3$ eV (approximately equal to the maximum temperature measured in figure 6 in the positive pulse afterglow), a magnetic field strength of $B = 10$ mT and $L = 5$ cm, taken from the magnetron field topology, we estimate $\tau_D \sim 1000$ μs. This is somewhat longer than the delay times measured. The exact mechanism for electron diffusion in the positive pulse period is unknown, however, if we can assume similar rates to those found during the on-time in other magnetron experiments [33, 34], namely Bohm diffusion, the diffusion coefficient can take the form,

$$D_B = \frac{1}{16} \frac{k_B T_e}{eB}$$

then the corresponding time to reach the measurement position is $\sim$130 μs. We see therefore combining the thermalisation and cross field diffusion times may explain the delay in measured heating effect after initiation of the positive pulse.

Our results show that increasing V_{pp} reduces the delay time in the observed rise in T_e. From figure 6, we see that for $V_{pp} = 300$ V, the delay time is $\sim$140 μs but for $V_{pp} = 200$ V it is $\sim$260 μs. At $V_{pp} = 100$ V it is longer than the positive pulse duration itself, or no heating occurs at all. Fast electron slowing down and equipartition times increase with increasing electron energy [32] however, the diffusion times for electrons across the B-field decrease. It seems from the measured trends (see figure 6), that the delay in local electron heating is more strongly governed by diffusion.

The fact that argon emission intensity increases and follows the electron temperature profile in the positive pulse indicates, that the hot electrons are exciting the neutral argon. The increased argon emission could be evidence of another discharge ignition, where now the target is positively biased, and the grounded walls act as an effective cathode. Hippler *et al* [18, 20] and Kozák *et al* [16], have also seen such a reappearance of background gas optical emission in the positive pulse and they too allude to the possibility of a reverse discharge where the electrons are returned to the cathode, gaining energy from the difference in potential between positive target and the local plasma.

We argue here that the observed electron heating does not originate from ohmic heating by electric fields in the plasma, since we do not see the presence of any (cathode directed) electron accelerating double layer structures created during application of the positive pulse. Such double layer structures are however seen in other magnetron systems operating under similar conditions [10, 12], responsible for ion acceleration towards the substrate.

The presence of wall re-sputtered material entering the discharge in the positive pulse phase of the bipolar pulse may lead to some unwanted contamination of the plasma, an effect that may dis-advantage the bipolar HiPIMS operation.

5. Conclusions

The temporal-evolution of electron temperature T_e, electron density n_e and argon and tungsten emission has been measured in bi-polar HiPIMS discharges using incoherent LTS and optical emission spectroscopy. The results show significant, but transient, electron heating takes place in the afterglow when a positive pulse or magnitude greater of equal to 200 V is applied. Rises in T_e are delayed with respect to the initiation of the positive pulse and decrease with positive voltage. This phenomenon is accompanied by evidence of excited metal species in the positive pulse region which are not present in the normal afterglow. Thomson scattering provides high fidelity electron property measurements with negligible perturbation to the plasma itself, making it a reliable unambiguous diagnostic tool. Emissive probe measurements also revealed that the plasma potential reaches values comparable to the target potential quickly at all positions measured, indicating no moving potential structure such as double layer is present in the plasma.

The observed effects in the positive pulse are understood in terms of the generation of a transient non-sustained ‘reverse’ discharge, in which secondary electrons generated at the grounded vessel walls due to ion bombardment heat the bulk electrons. The large wall sheath potentials also lead to re-sputtered tungsten entering the discharge. Such a contaminating effect may not be an ideal feature in bipolar HiPIMS operation.

Acknowledgments

This work was supported by the Engineering and Physical Sciences Research Council (Grant EP/L01663X/1).

Data availability statement

All data that support the findings of this study are included within the article (and any supplementary files).

ORCID iDs

Marcus A Law https://orcid.org/0000-0002-2165-5503
Francis Lockwood Estrin https://orcid.org/0000-0002-1922-1124
Mark D Bowden https://orcid.org/0000-0003-4128-4823
James W Bradley https://orcid.org/0000-0002-8833-0180

References

[1] Lundin D, Minea T and Gudmundsson J T 2019 *High Power Impulse Magnetron Sputtering: Fundamentals, Technologies, Challenges and Applications* (Amsterdam: Elsevier)
[2] Samuelsson M, Lundin D, Jensen J, Raadu M A, Gudmundsson J T and Helmersson U 2010 *Surf. Coat. Technol.* **205** 591–6
[3] Paulitsch J, Schenkel M, Zufraß T, Mayrhofer P H and Münz W-D 2010 *Thin Solid Films* **518** 5558–64
[4] Magnus F, Ingason A S, Sveinsson O B, Olafsson S and Gudmundsson J T 2011 *Thin Solid Films* **520** 1621–4
[5] Anders A 2010 *J. Vac. Sci. Technol.* A **28** 783–90
[6] Nakano T, Murata C and Baba S 2010 *Vacuum* **84** 1368–71
[7] Wu B, Haehnlein I, Shchelkanov I, McLain J, Patel D, Uhlig J, Jurczyk B, Leng Y and Ruzic D N 2018 *Vacuum* **150** 216–21
[8] Viloan R P B, Gu J, Boyd R, Keraudy J, Li L and Helmersson U 2019 *Thin Solid Films* **688** 10
[9] Tiron V, Ursu E-L, Cristea D, Munteanu D, Bulai G, Ceban A and Velicu I-L 2019 *Appl. Surf. Sci.* **494** 871–9
[10] Velicu I-L, Ianoş G-T, Porosnicu C, Mihăilă I, Burducea I, Velea A, Cristea D, Munteanu D and Tiron V 2019 Energy-enhanced deposition of copper thin films by bipolar high power impulse magnetron sputtering *Surf. Coat. Technol.* **359** 97–107
[11] Santiago J A, Fernández-Martínez I, Kozák T, Capek J, Wennberg A, Molina-Aldareguia J M, Bellido-González V, González-Arrabal R and Monclús M A 2019 *Surf. Coat. Technol.* **358** 43–9
[12] Tiron V and Velicu I L 2020 *Plasma Sources Sci. Technol.* **29** 015003
[13] Block L P 1978 *Astrophys. Space Sci.* **55** 59–83
[14] Charles C 2007 *Plasma Sources Sci. Technol.* **16** R1–R25
[15] Keraudy J, Viloan R P B, Raadu M A, Brenning N, Lundin D and Helmersson U 2019 *Surf. Coat. Technol.* **359** 433–7
[16] Kozák T, Pajdarová A D, Čada M, Hubička Z, Mareš P and Čapek J 2020 *Plasma Sources Sci. Technol.* **29** 065003
[17] Avino F, Sublet A and Taborelli M 2019 *Plasma Sources Sci. Technol.* **28** 01LT03
[18] Hippler R, Cada M, Stranak V and Hubicka Z 2019 *Plasma Sources Sci. Technol.* **28** 115020
[19] Hippler R, Cada M and Hubicka Z 2020 *Appl. Phys. Lett.* **116** 064101
[20] Hippler R, Cada M and Hubicka Z 2020 *J. Appl. Phys.* **127** 203303
[21] Britun N, Michiels M, Godfroid T and Snyders R 2018 *Appl. Phys. Lett.* **112** 234103
[22] Pajdarová A D, Kozák T, Hubička Z, Čada M, Mareš P and Čapek J 2020 *Plasma Sources Sci. Technol.* **29** 085016
[23] van de Sande M 2002 Laser scattering on low temperature plasmas: high resolution and stray light rejection *PhD Thesis* Eindhoven University of Technology, Eindhoven
[24] Tsikata S, Vincent B, Minea T, Revel A and Ballage C 2019 *Plasma Sources Sci. Technol.* **28** 03LT02
[25] Ryan P J, Bradley J W and Bowden M D 2019 *Phys. Plasmas* **26** 073515
[26] Ryan P J, Bradley J W and Bowden M D 2019 *Phys. Plasmas* **26** 040702
[27] Muraoka K, Uchino K and Bowden M D 1998 *Plasma Phys. Control. Fusion* **40** 1221
[28] Mishra A, Kelly P J and Bradley J W 2010 *Plasma Sources Sci. Technol.* **19** 045014
[29] Kozák T and Lazar J 2018 *Plasma Sources Sci. Technol.* **27** 115012
[30] Hnilica J, Klein P, Vašina P, Snyders R and Britun N 2020 *J. Appl. Phys.* **128** 043303
[31] Yang X and Hassanein A 2014 *Appl. Surf. Sci.* **293** 187–90
[32] Spitzer L 1956 *Physics of Fully Ionized Gases* (New York: Interscience)
[33] Rossnagel S M and Kaufman H R 1987 *J. Vac. Sci. Technol.* A **5** 88–91
[34] Brenning N, Merlino R L, Lundin D, Raadu M A and Helmersson U 2009 *Phys. Rev. Lett.* **103** 225003